Chapter 14

Muscarinic Receptor Gene Transfections and In Vivo Dopamine Electrochemistry: Muscarinic Receptor Control of Dopamine-Dependent Reward and Locomotion

Stephan Steidl, David Ian Wasserman, Charles D. Blaha, and John Yeomans

Abstract

Cholinergic neurons in laterodorsal (LDT) and pedunculopontine (PPT) tegmental nuclei respond to novel, arousing stimuli, then directly activate dopamine neurons, and increase dopamine outputs as measured by either in vivo microdialysis or by electrochemistry (described here). These mesopontine cholinergic neurons also directly activate superior colliculus and thalamic systems important for attention to novel stimuli, and for reward-seeking behaviors. M_5 muscarinic receptors that activate dopamine neurons and reward-seeking behaviors have been studied using pharmacology, knockout mice, oligonucleotide knockdown, and with electrochemistry and Herpes simplex viral gene transfections (HSV-M_5) protocols described here. Protocols for using HSV-M_5 genes, and designed M_4D and M_3D muscarinic receptor genes in behaving mice and for dopamine electrochemistry are presented, along with consequences for drug and gene therapy.

Key words Chronoamperometry, Viral transfections, DREADDs, Gene therapy, HSV, AAV, Reward, Locomotion, M_5 muscarinic receptors, Dopamine

1 Background and Historical Overview

Dopamine neural output is important for human diseases, such as Parkinson's, schizophrenia, and drug abuse. Drugs that influence dopamine output have powerful effects on behaviors in animals (such as locomotion, reward seeking, and motor control) and similarly powerful effects on confidence, mood and motor control in humans important for the therapeutic value of pharmaceuticals. We have studied how dopamine neural outputs and reward-seeking behaviors in rodents are influenced by cholinergic and GABAergic neurons of the midbrain and pons, and then how M_2, M_3, M_4, and especially M_5 muscarinic receptors and gene manipulations influence dopamine efflux and behaviors.

Jaromir Myslivecek and Jan Jakubik (eds.), *Muscarinic Receptor: From Structure to Animal Models*, Neuromethods, vol. 107,
DOI 10.1007/978-1-4939-2858-3_14,

1.1 Localization of Muscarinic M_5 mRNA and Receptors in the Rodent Brain

The m5 receptor gene was discovered by Bonner's group [1], shortly after the identification of m1–m4 genes. Complete maps of m1–m5 mRNA expression are now available on the Allen Mouse Brain Atlas. Regional localization of M_1–M_5 proteins in brain stem has been reviewed [2].

Immunoprecipitation studies show that M_5 receptors account for only about 1 % of all muscarinic receptors in the rat brain. Low receptor numbers make it difficult to localize M_5 receptors by immunohistochemistry [3, 4]. Expression of m5 mRNA is localized to ventral tegmental area (VTA) and substantia nigra, zona compacta (SNc). Following 6-hydroxydopamine dopamine lesions m5 mRNA is no longer detected in midbrain [5, 6]. This suggests that excitatory M_5 receptors are important for activation of dopamine neurons, and inspired the creation of M_5 knockout (M_5-KO) mice [7, 8].

1.2 Muscarinic Receptors in VTA Activate Dopamine Rewards

Cholinergic input to dopamine reward systems was first studied using VTA microinjections in rats bar-pressing for rewarding hypothalamic brain stimulation. Microinjections of acetylcholine, nicotine or carbachol into the VTA were found to increase sensitivity to rewarding brain stimulation [9–11], as well as to increase mesolimbic dopamine efflux [12]. Microinjections of muscarinic antagonists into the VTA were found to reduce sensitivity to rewarding brain stimulation more than nicotinic antagonists [13]. Similarly, selective knockdown of M_5 muscarinic receptors with antisense oligonucleotides in the VTA reduced sensitivity to rewarding brain stimulation [14].

Food- and opioid-motivated rewards were also strongly reduced by these same muscarinic antagonists in the VTA [15, 16]. Acetylcholine levels in VTA are increased during eating, drinking and brain-stimulation rewards as measured by in vivo microdialysis [17].

1.3 Ch5 and Ch6 Cholinergic Neurons Activate Dopamine Neurons

Cholinergic neurons (Ch1–8) are defined by the presence of the synthesizing enzyme choline acetyltransferase (ChAT) [18]. The only direct projections of cholinergic neurons to the VTA and SNc are from pedunculopontine (PPT; Ch5) and laterodorsal tegmental nuclei (LDT; Ch6) [19, 20]. The direct projections to VTA dopamine neurons from these nuclei are especially from LDT and caudal PPT cholinergic and glutamate neurons [21, 22]. The Ch5/Ch6 cholinergic projections to VTA and SNc are less dense than to thalamus or superior colliculus intermediate layers, however.

These anatomical connections suggest that cholinergic activation of dopamine systems is part of a larger cholinergic arousal system [2]. So, novel and rewarding stimuli activate fast saccadic eye movements and approach turns via the superior colliculus, facilitated by nicotinic input from Ch5 [23, 24]. At the same time, Ch5/6 cholinergic activation of thalamus facilitates cortical arousal

and attention to these stimuli [25] via fast nicotinic and slower M_1-type muscarinic receptors [26, 27]. Ch5 and Ch6 neurons also provide weaker anatomical projections to Ch1–4 basal forebrain nuclei supporting cortical arousal [28–30]. Finally, SNc and VTA dopamine activation provides sustained motor arousal and motivated reward-seeking behaviors.

Excitotoxic lesions of PPT and LDT neurons reduce behavioral arousal and reward sensitivity in several ways. For example, bilateral lesions of caudal PPT block acquisition of brain-stimulation reward [31] and morphine conditioned place preference [32]. Cholinergic output can be inhibited pharmacologically in PPT or LDT by local infusion of the cholinergic agonist carbachol, which inhibits Ch5 and Ch6 neurons via M_2 and M_4 inhibitory receptors [33, 34]. Carbachol in the PPT similarly inhibits dopamine output [35], brain-stimulation reward or locomotion [36, 37]. By contrast, muscarinic antagonists in the PPT or LDT strongly facilitate dopamine outputs, rewarding brain stimulation, or locomotion, apparently via M_2 receptors [38]. M_4 receptors in VTA also appear to inhibit ACh release from VTA cholinergic terminals [39].

1.4 Mesopontine Activation of Dopamine Output via M_5 Muscarinic Receptors in Tegmentum

In vivo electrochemistry allows temporal resolution of the many different neural pathways and receptors that influence dopamine transmission (e.g., ref. 38). Following LDT or PPT electrical stimulation (see Protocol and Fig. 1) dopamine levels change in three phases in rats: (1) Dopamine increases for 2–4 min due to both VTA nicotinic and AMPA glutamate receptors, (2) Dopamine decreases for 5–10 min due to LDT/PPT M_2-like receptors, followed by (3) sustained increases in dopamine (from 10 to 60 min post stimulation), due to M_5 muscarinic receptors in VTA or SNc [38, 40]. The third phase is completely removed by muscarinic receptor antagonists infused into the VTA or SNc, or by m5 gene knockout (Fig. 1a; [38, 40–42]). Therefore, M_5 receptors on dopamine neurons have very long-lasting and powerful activating effects on dopamine outputs to the nucleus accumbens and striatum.

Although excitatory M_3 receptor mRNA is found near orexin/hypocretin neurons in the lateral hypothalamus, carbachol inhibits, and the M_3 antagonist 4-DAMP excites, orexin neurons [43]. Therefore M_3 receptors may excite GABA interneurons in the hypothalamus as they do in midbrain near dopamine neurons [44].

2 Electrochemical Methods to Study Muscarinic Modulation of Brain Dopamine Signaling

Oxidization of an electroactive compound such as dopamine results in measurable current flow (Fig. 1b bottom). The methods outlined below describe an experimental setup that uses chronoamperometry

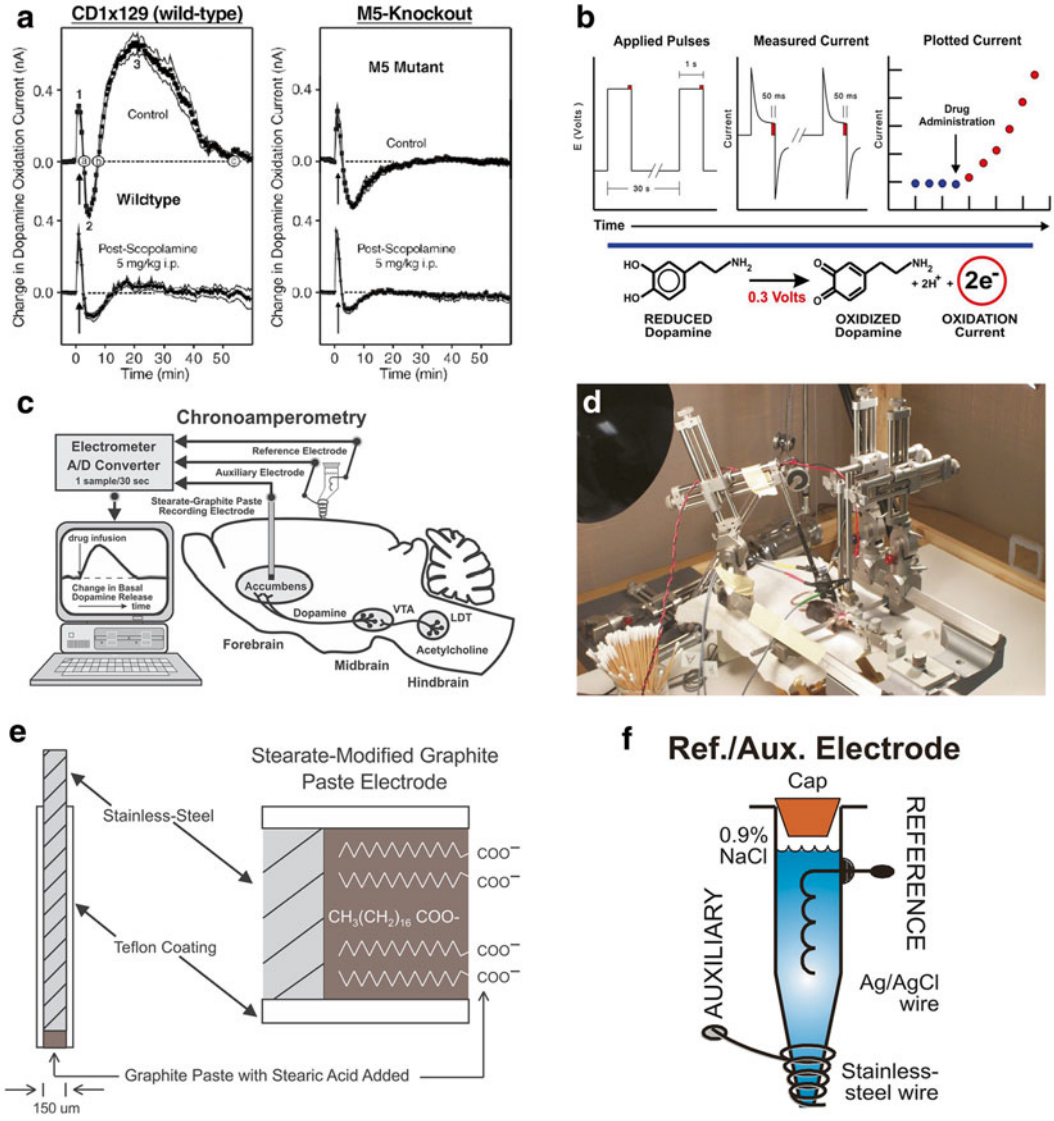

Fig. 1 (**a**) Nucleus Accumbens (NAc) Dopamine Efflux Measured by Chronoamperometry in Mice after Electrical Stimulation of the LDT (*arrow*). *Left Panel Top*: In wild-type mice LDT stimulation induces a rapid increase in NAc dopamine (1) followed by a decrease in dopamine efflux from 3 to 8 min (2). Dopamine efflux is again increased from 10 to 60 min following LDT stimulation (3). *Left Panel Bottom*: Systemic pretreatment with the muscarinic receptor antagonist scopolamine in wild-type mice selectively blocks the third phase of increased dopamine efflux. *Right Panel*: In M_5 knockout mice the third phase of increased dopamine efflux following LDT electrical stimulation is completely absent and is not further reduced by systemic scopolamine pretreatment (Figure adapted from [41]). (**b**) In chronoamperometry the applied potential to the working electrode is near-instantaneously stepped up from a resting potential to a value above the dopamine oxidation potential (−0.15 V to 0.25 V) for 1 s duration at a fixed interval. To measure dopamine with carbon paste electrodes, the potential is instantly stepped from a resting value of −0.15 V to 0.25 V for 1 s, every 30–60 s (*left*). As the potential is stepped up, the recorded current increases dramatically, and this is due to charging current of the electrode and oxidation of the electroactive species. The charging current decays as the potential is held, and the faradaic (i.e., dopamine oxidation) current (*bottom*) is measured and integrated over the final 50 ms of the 1000 ms pulse (*middle*; [45]). Oxidation current is then plotted across time. Dopamine oxidation current is proportional to in vivo dopamine concentration (*right*). (**c**) Chronoamperometry in combination with carbon paste electrodes to measure in vivo dopamine: the stearate-modified graphite paste recording electrode is implanted in the

(one of several available electrochemical techniques) in combination with stearate-modified graphite paste electrodes to measure dopamine in vivo. Three electrodes are needed: the working electrode is implanted into the brain area of interest (see section 2.2.2) and a combined reference and auxiliary electrode is placed into contact with the cortex (see section 2.2.3). A potentiostat, or electrometer, provides a circuit between the three electrodes and allows for the application of a voltage to the recording electrode via the auxiliary electrode, as well as the maintenance of a potential difference between the recording and reference electrodes (Fig. 1c; [45]). When a positive voltage of sufficient amplitude is applied to the working electrode it causes the oxidation of electroactive compounds (e.g., dopamine) at its surface. Oxidation results in the transfer of electrons producing a measurable current (Fig. 1b bottom). The current flow, termed the faradaic current, is proportional to the concentration of the neurochemical of interest [45, 46]. In chronoamperometry the applied potential is near-instantaneously stepped from a resting value of −0.15 V to 0.25 V for 1 s, every 30–60 s. The faradaic (i.e., oxidation) current is measured and integrated over the final 50 ms of the 1000 ms pulse (Fig. 1b; [45]).

2.1 Materials

2.1.1 Stereotaxic Equipment

1. Stereotaxic frame (Model 1504 with Model 1211 base plate; this stereotaxic frame allows for the use of 3–4 manipulator arms simultaneously), mouse or rat nose bar and rat ear bars (model 855) produced by David Kopf Instruments (Fig. 1d).
2. Stereotaxic drill (Model 1471 with Model 1469 stereotaxic holder) produced by David Kopf Instruments and trephine drill bits (Harvard Apparatus).
3. Stereotaxic cannula holder (Model 1776-P1) produced by David Kopf Instruments.

Fig. 1 (continued) brain area of interest (e.g., the nucleus accumbens), a combined reference and auxiliary electrode is placed into contact with the cortex (opposite hemisphere). A potentiostat, or electrometer, provides a circuit between the three electrodes and allows for the application of a voltage potential to the recording electrode via the auxiliary electrode, as well as the maintenance of a potential difference between the recording and reference electrode [45]. When a positive voltage is applied to the working electrode of sufficient amplitude it causes the oxidation of dopamine at its surface. (**d**) Anesthetized animal recordings should be performed in a standard Faraday cage. Place the stereotaxic apparatus inside the cage and place the electrometer outside of the cage. The stereotaxic apparatus shown here allows for the use of 3–4 manipulator arms simultaneously. At minimum, one carrier is needed to hold the stearate-modified graphite paste recording electrode and a second carrier is needed to hold the combined reference and auxiliary electrode. Additional carrier arms then allow for mounting stimulating electrodes (i.e., for PPT/LDT electrical stimulation) or injection cannulae (for intracranial microinjection of drugs or pharmacological agents). (**e**) Stearate-modified carbon paste electrode constructed from a Teflon-coated stainless steel wire. Extruding the Teflon coating ~1 mm beyond the tip of the stainless-steel wire creates a well that is filled with stearate-modified graphite paste. (**f**) Diagram showing a combined reference/auxiliary electrode

4. Various surgical instruments: scalpel, forceps, small animal clippers etc. (Fine Science Tools).
5. Hamilton syringes (Model 7002KH), injector tubing, guide cannulae (26 gauge), injector cannulae (33 gauge; Plastics One Inc.) and a micro-infusion pump (Harvard Apparatus).
6. Various surgical supplies: gauze, cotton tip applicators, betadine, latex gloves, etc.
7. Urethane for anesthesia (Sigma-Aldrich).
8. Temperature-regulated heating pad (e.g., TC-1000; CWE Inc., New York, NY).

2.1.2 Equipment for Construction of Stearate-Modified Graphite Paste Recording Electrodes and Reference/Auxiliary Electrodes

1. Glass mortar and pestle, a 25 ml beaker, a 250 ml beaker, appropriately sized magnetic stir bar, a glass capillary heat-sealed on one end, and a stirring hotplate.
2. Stearate (99.9 % purity), silicone oil, and graphite powder (particle size < 10 μm; all available from Sigma-Aldrich), 0.9 % saline solution.
3. Teflon-coated stainless-steel wire (0.008″ o.d.; Medwire, Mount Vernon, NY), silver wire (0.008″ o.d.; A&M Systems Sequim WA), stainless steel wire (0.008″ o.d.; A&M Systems Sequim WA).
4. #5 forceps, a glass plate, masking tape, #10 scalpel blade, Teflon tape, a compound microscope that will allow for viewing of the electrode tip, a 9 V battery, black wax, a needle tip, standard 1 ml pipette tip, epoxy.

2.1.3 Materials for In Vitro Calibration of Graphite-Paste Electrodes

1. 0.01 M phosphate-buffered saline solution, dopamine hydrochloride, perchloric acid (Sigma-Aldrich), and double distilled water.

2.1.4 Materials for In Vivo Electrochemical Recordings in Anesthetized Rats or Mice

1. Bipolar concentric stimulating electrode (e.g., SNE-100, Rhodes Medical Co., Woodland Hills, CA or CBARD75, FHC, Bowdoin, ME).
2. Programmable pulse generator (e.g., Master 9, AMPI, Jerusalem, Israel) connected to a stimulus isolator (e.g., ISO-Flex, AMPI, Jerusalem, Israel) to apply stimulation current pulses.
3. Electrometer (e.g., EChempro, GMA Technologies, Vancouver, Canada).

2.2 Methods

2.2.1 Preparation of Stearate-Modified Graphite Paste

Graphite paste electrodes are treated to enhance selectivity for dopamine by incorporating a fatty acid (stearic acid) into the graphite paste [46, 47]. The fatty acid provides an anionic recording surface that slows down the electron transfer kinetics of anions (i.e., ascorbic acid and dopamine metabolites, such as DOPAC [45]).

1. Using the 25 ml glass beaker and stir bar dissolve 75 mg of stearate in 1 ml silicone oil heated to 40 °C (Note 1).

2. Once the stearate crystals are fully dissolved remove from heat and transfer contents of beaker into glass mortar. Add 1 g of graphite powder and thoroughly mix using the glass pestle. The consistency of the mixture will start off paste-like and with additional mixing will become powdery.
3. Transfer stearate-modified graphite paste to a light-proof glass vial for storage.

2.2.2 Construction of Stearate-Modified Graphite Paste Recording Electrodes

1. Cut a length of Teflon-coated stainless-steel wire from the spool using wire cutters. Trim the length of wire to ~10 cm using a #10 scalpel blade. Straighten the cut length of wire carefully.
2. Strip ~1 cm of Teflon coating form one end of the wire. This will provide the top end of the implantable electrode where the electrometer can be connected.
3. Use a pair of #5 forceps to grip exposed 1 cm length of stainless-steel wire. Holding the electrode by the forceps, gently pass the coated portion between thumb and forefinger to loosen the Teflon coating. Be careful not to pull the Teflon coating off the stainless-steel wire.
4. Extrude the Teflon coating 2–3 mm past the tip of the stainless-steel wire on the opposite end.
5. While holding the uncoated portion of the wire between the thumb and forefinger of one hand, lay the wire flat on the glass plate, maintaining a loose grip on the wire. Use a thin-edged razor blade to cut the well's surface. Hold the blade perpendicular to the wire approximately 5 mm behind the end of the stainless-steel wire on the end where you previously extruded the Teflon coating. Gently lower the blade onto the wire and let blade rotate the wire across the glass surface for one full rotation. Remove the excess Teflon using forceps.
6. Hold the stainless-steel wire at the electrode contact end in one hand. Then with the thumb and forefinger of the other hand around the center of the electrode gently push the remaining Teflon coating so that the edge of the well extrudes ~1 mm beyond the tip of the wire (Fig. 1e). Examine the well surface under a microscope. The well should have a clean and unblemished concentric Teflon surface. And uneven cut will create Teflon spirals visible under the microscope. If this occurs cut another well as described above.
7. Grip and hold the wire firmly using #5 forceps at a distance from the well surface that is about 2–3 mm over the depth the electrode is to be implanted (~1 cm for a mouse). Loop the wire tightly around the tip of the forceps for two complete revolutions. Carefully slide out the tip of the forceps. Wrap a small (3–4 mm wide × 2 cm long) strip of masking tape around the loop.

8. Place a small quantity of the stearate-modified graphite paste mixture onto the clean surface of a glass plate. If needed clean the glass surface with ethanol. Holding the electrode around the contact end between thumb and forefinger gently push the well into the graphite paste mixture to fill the well. Avoid large particles of graphite powder and do not apply pressure as this will crush the fragile well.
9. Clean the excess paste from the well's side and surface by gently rubbing the tip across a suspended piece of Teflon tape.
10. Then, hold the electrode perpendicular to the glass surface (well facing down) and drop the electrode onto the glass surface to tightly pack the graphite paste into the Teflon well (Fig. 1e).
11. Examine the electrode's surface under a microscope. The graphite surface should appear shiny and smooth and the walls of the well's surface should be free of graphite. If cracks or grooves are observed additional packing and/or additional graphite paste may be required (Note 2).

2.2.3 Construction of Reference/Auxiliary Electrode (Fig. 1f)

1. Use gloves to handle silver wire. Wrap a length of silver wire (~10 cm) around the shaft of a stereotaxic drill bit to achieve about 10–15 closely spaced, but not touching, loops.
2. Place the coil in the 250 ml beaker filled with 0.9 % saline ensuring the entire coil is submerged. Attach the coil to the anode (+) of the 9 V battery. Attach a second short length of bare silver wire to the cathode (−) of the battery. The process of silver chloriding the wire will darken the surface of the coil. Set aside the coil in saline until ready for use.
3. Obtain a standard 1 ml pipette tip. Use a heated 18 g needle tip to burn a hole into the side of the pipette tip ~1 cm from the top rim. Next, melt a circular groove around the circumference of the pipette tip at the level of the hole. Melt a second circular groove just above where the pipette tip tapers.
4. Insert the silver/silver chloride coil into the pipet and feed the excess wire on one end through the hole. Cover the hole with black wax to secure the position of the coil.
5. Obtain a 30 cm piece of stainless-steel wire and tightly wrap it around the exposed piece of Ag/AgCl wire. Then wrap this wire around the pipette (starting in the groove) and a closely placed dowel to form a loop. This will provide a contact for the electrometer to connect to the Ag/AgCl reference electrode.
6. Obtain a second 30 cm piece of stainless-steel wire. Coil this wire around the groove created just above the tapered end of the pipette tip leaving plenty of access on one end. Start looping the wire downward to the tip creating a coil on the way down. Wind the wire around the groove at the tip several times

and begin looping upward again to the middle groove. Wrap around the middle groove several times and twist remainder around the other end of the wire left in place previously. Then wrap this wire around the pipette and a closely placed dowel to form a loop. This will provide a contact for the electrometer to connect to the auxiliary electrode. Cover the middle groove and wire with epoxy to ensure the position of the auxiliary electrode is secure.

7. Fill interior of pipette with 0.9 % saline while epoxy is drying. Insert an appropriately sized rubber stopper in the top end of the pipette tip (Fig. 1f). Set aside until ready to use (Note 3).

2.2.4 In Vitro Testing of Graphite Paste Electrodes

1. Place a glass container containing 15 ml of a 0.01 M phosphate-buffered saline solution on a battery-operated magnetic stirrer.
2. Submerge the graphite paste electrode and the combination reference/auxiliary in the solution.
3. Use the electrometer to obtain a linear sweep voltammogram by ramping the potential applied to the working electrode from −0.15 V to 0.5 V vs. the Ag/AgCl electrode at a rate of 10 mV/s.
4. Add discrete quantities of a 2 mM solution of dopamine (37.9 g of dopamine hydrochloride dissolved in 90 ml double distilled water and 10 ml of 0.1 M perchloric acid) to achieve a 1 μM concentration of dopamine in the phosphate-buffered saline solution. Stir the solution gently for a period of 5 s (Note 4).
5. Obtain another linear sweep voltammogram. Repeat the process for between 3 and 5 additions of 1 μM dopamine to confirm, first, that peak current was always obtained at the same potential and, second, that the relative increases in peak current were consistent across consecutive 1 μM additions of dopamine.

2.2.5 In Vivo Electrochemical Recordings in Anesthetized Rats or Mice

1. Anesthetized animal recordings should be performed in a standard Faraday cage. Place the stereotaxic apparatus inside the cage. Place the electrometer outside of the cage.
2. Anesthetize mice or rats with urethane (1.5 g/kg, i.p.; initial dose supplemented with 0.3 g/kg 30 min later).
3. Secure mouse or rat in a stereotaxic frame. Maintain body temperature at 37 ± 0.5 °C with a temperature-regulated heating pad.
4. Drill a hole into the skull above the brain area of interest (e.g., NAc or dorsolateral striatum) large enough to accommodate the graphite paste recording electrode. Drill a second larger hole to accommodate the tip of the combined reference/auxiliary electrode. This hole should be placed so that the

combined reference/auxiliary electrode is in contact with the opposite brain hemisphere at a distance that does not interfere with placement of the recording electrode.

5. Mount the combined reference/auxiliary electrode on a stereotaxic carrier and connect the electrometer. Ensure the reference/auxiliary electrode is completely filled with 0.9 % saline (air bubbles commonly occur at the tip). Place a drop of saline on to the hole and place the reference/auxiliary electrode into contact with the cortical surface.
6. Attach the graphite paste recording electrode to another stereotaxic carrier and lower into the brain area of interest (e.g., NAc) according to coordinates obtained from a stereotaxic brain atlas. Ensure that the tip of the electrode does not come into contact with blood.
7. Attach the electrometer to the recording electrode (Fig. 1d).
8. Perform repetitive chronoamperometric measurements of oxidation current by applying potential pulses from –0.15 to 0.30 V to the recording electrode (vs. reference electrode) for 1 s duration at 30 or 60 s intervals.

2.2.6 Using Muscarinic Knockout Mice to Study the Role of Muscarinic Receptor Signaling in Mesopontine Excitation of Mesolimbic or Nigrostriatal Dopamine Signaling

1. Obtain muscarinic receptor knockout mouse and wild-type controls (available from Taconic Bioscience, Inc.).
2. Secure anesthetized mouse in stereotaxic frame as described above.
3. Drill an additional hole into the skull above the LDT or PPT and lower a bipolar concentric stimulating electrode into either LDT or PPT. Use a programmable pulse generator connected to a stimulus isolator to apply current pulses with the following parameters: 1 s, 35 Hz train of 400 μA pulses (1 s intertrain interval) applied over a 60 s period (1050 pulses in total). These parameters are designed to mimic spontaneous firing patterns of PPT neurons in awake, naturally aroused animals [25].
4. Comparisons of electrically evoked nucleus accumbens or dorsal striatum dopamine efflux between wild-type and knockout mice will reveal the contribution of muscarinic receptors to each of the three phases of dopamine efflux [41].

2.2.7 Using In Vivo Pharmacology to Study the Role of Midbrain Muscarinic Receptor Signaling in Mesopontine Excitation of Mesolimbic or Nigrostriatal Dopamine Signaling

1. Secure anesthetized mouse or rat in stereotaxic frame as described above.
2. Drill an additional hole above the VTA (when studying LDT electrically evoked nucleus accumbens dopamine efflux) or the SNc (when studying PPT electrically evoked dorsal striatal dopamine efflux) to allow for insertion of a guide cannula. The guide cannula can be held by a stereotaxic carrier or can be chronically implanted by securing it to the skull surface using a combination of stainless-steel jeweler's screws and dental cement.

3. Apply electrical stimulation to the LDT or PPT and observe the triphasic response pattern [38, 40–42].
4. Infuse a muscarinic receptor antagonist, or vehicle, into the VTA or SNc (Note 5) and repeat electrical stimulation.
5. Compare the predrug, vehicle-treated, and antagonist-treated response patterns to determine the contributions of muscarinic receptors.

2.3 Notes

1. Be careful not to overheat the silicone oil. This is easily accomplished by removing the beaker from the heat source the moment the last few crystals of stearate are observed to dissolve into the silicon oil.
2. The microscope should allow for viewing the tip of the graphite paste electrode. Wells have to be recut or repacked if necessary.
3. The saline solution that fills the pipette tip should be replaced regularly. When not in use the tip of the reference/auxiliary electrode should be submerged in saline solution.
4. Prepare fresh dopamine solution for in vitro calibration.

3 Opioid Rewards and Mesopontine/M_5 Activation of Dopamine Neurons

M_5-KO mice show deficits in responding to morphine, either in conditioned place preference or in morphine-induced locomotion tasks, but not stimulant- or saline-induced locomotion tasks [48–51]. Similarly, PPT or LDT lesions significantly reduce morphine-induced dopamine release [52, 53]. Finally, M_5-KO mice lose their dopamine response to morphine entirely [42]. This suggests that morphine acts indirectly through the PPT/LDT to M_5 pathway to activate dopamine neurons, and for dopamine-dependent behavioral effects of morphine.

These effects of morphine depend on μ-opioid receptors in the ventral tegmental region that inhibit GABA neurons. The most critical GABA neurons for opioid rewards and for morphine-induced locomotion are located just caudal to VTA in the rostromedial tegmental nucleus (RMTg; [22, 54]). RMTg GABA neurons express together μ-opioid, nociceptin, $GABA_A$ and M_4 muscarinic receptors, all of which are normally inhibitory. We have proposed that together these receptors inhibit GABA neurons and thereby disinhibit cholinergic and dopaminergic output neurons needed for opioid reward and dopamine effects [55].

To excite VTA and RMTg neurons, we infused HSV-M_5-GFP bilaterally into M_5-KO and wild-type mice (Fig. 2) (See protocol below). Viral infections work best when infecting cells, not axons, due to the larger surface area of dendrites and somata which clearly

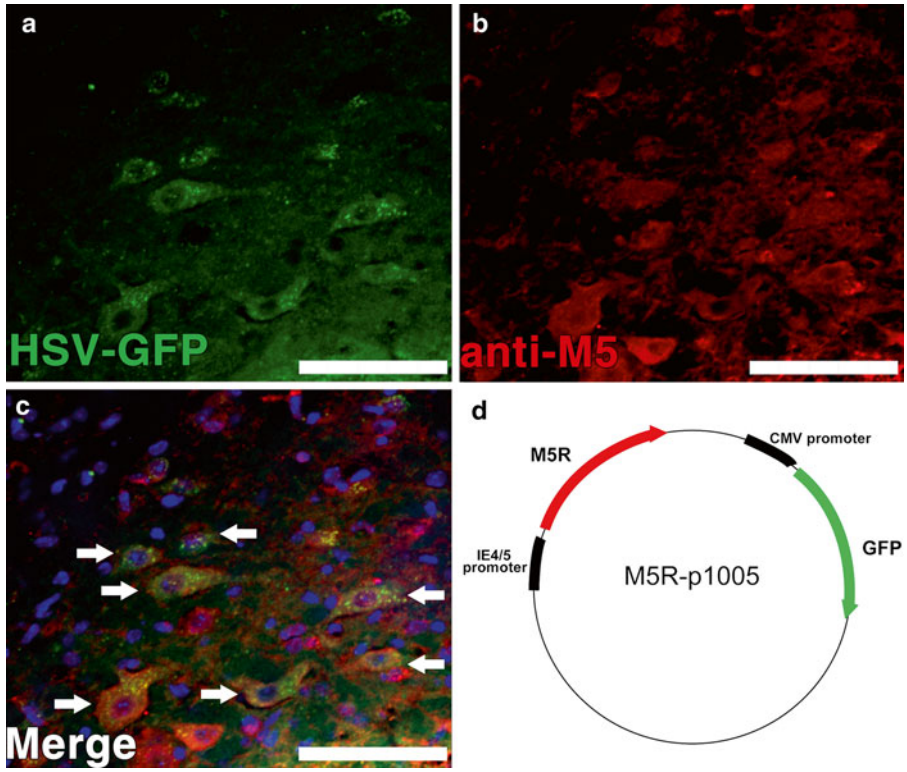

Fig. 2 (**a–c**) HSV-M_5-GFP Transfected Neurons and M_5 Expression. The HSV-M_5-GFP vector was infused into VTA sites in M_5-KO mice. Expression of viral GFP can be seen in (**a**). Sections were double-labeled with M_5 antibodies (*red*: **b**) and DAPI. (**c**) Merged image displaying triple-labeled cells (*purple nucleus*, with *yellow spots* in cytosol) of viral GFP, M_5-expression, and DAPI (20× magnification, bar represents 75 μm) All cells labeled with viral GFP were also M_5 positive (*white arrows* indicate triple-labeling). As the mouse was an M_5 knockout, all observed M_5 expression was virally mediated. (**d**) Schematic of the M_5R-p1005 Vector. Expression of M_5R was driven by a constitutive IE4/5 promoter while GFP expression was driven by a CMV promoter. Replication-deficient Herpes simplex virus (*HSV*)-derived particles were made from this vector as previously described ([60]; Figure modified from [22])

express GFP after viral transfections (Fig. 2a–c). This HSV-M_5 method relies on expression of extra M_5 receptors, so that endogenous activation of cholinergic neurons and endogenous ACh release is needed to activate the M_5 receptors.

Although these two sites are less than 1 mm apart, VTA infections strongly facilitated morphine-induced locomotion, while RMTg infections blocked morphine-induced locomotion (Fig. 3). Both VTA and RMTg sites receive direct projections from many LDT and caudal PPT cholinergic neurons [55]. Therefore, the same populations of PPT and LDT neurons that excite VTA and SNc neurons via M_5 muscarinic receptors can simultaneously inhibit RMTg GABA neurons via inhibitory muscarinic M_4 receptors. This suggests that morphine-mediated inhibitory inputs

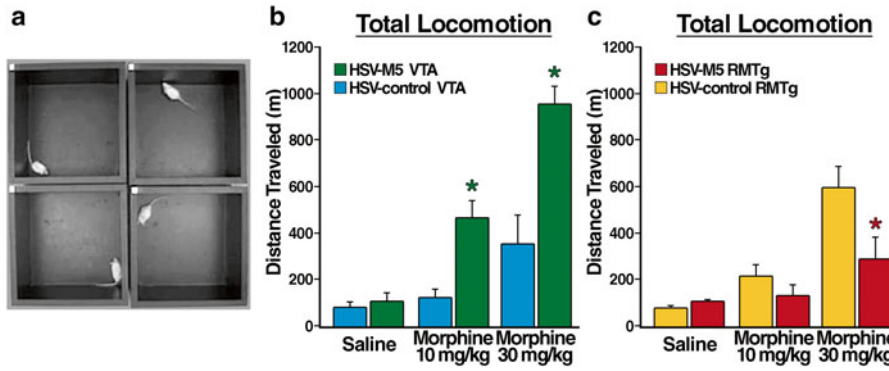

Fig. 3 (**a**) Open-field apparatus for locomotion. Mice were placed in the center of arenas while a video camera recorded their horizontal movements. A computerized tracking program, Noldus Ethovision, thereafter scored the video and calculated the distance traveled. (**b–c**) Total saline and morphine-induced locomotion following HSV transfections. (**b**) In VTA, HSV-M_5 infusions (*green*) significantly increased distance traveled at both morphine doses over HSV-control vector (*blue*) over the 2 h period. No differences were observed for saline. (**c**) In RMTg, HSV-M_5 infusions (*red*) significantly reduced total locomotion over HSV-control vector (*orange*) only at 30 mg/kg. (M_5-VTA, $n=7$; M_5-RMTg, $n=15$; Control-VTA, $n=6$, Control-RMTg, $n=7$.) (figure modified from [55])

to RMTg are facilitated by M_4 inhibition at the same time that cholinergic activation of dopamine neurons occurs. Then RMTg GABA connections to PPT and VTA release these neurons from inhibition to facilitate the arousing and rewarding outputs of cholinergic and dopaminergic systems. Therefore, the critical roles of RMTg inputs, and of caudal PPT, LDT and M_5 receptor outputs, to opioid reward and locomotion, appear to depend on close interconnections, supported by appropriate muscarinic receptor modulations.

These muscarinic effects can be studied by local site-specific viral transfections of neurons, or by neuron-specific viral transfections, using TH::Cre, ChAT::Cre or GAD2::Cre mouse lines. To identify which RMTg GABA neurons are critical for morphine-induced locomotion, we used AAV-M_3D and AAV-M_4D to activate or inhibit mCherry-labeled GABA RMTg neurons in GAD2::Cre mice. This method for activating genetically modified muscarinic receptors (i.e., M_3D for excitation like M_5, and M_4D for inhibition like M_4) relies on exogenously administered clozapine-N-oxide (CNO) [56]. AAV induces long-term infections of identified neurons, while systemic CNO control of these neurons occurs via muscarinic receptors with mutant binding sites. For future gene therapy applications, this is a powerful method for remote control of specifically targeted brain neurons (see protocol below).

4 Local Gene Control with HSV-M_5-GFP Viral Transfections Including Cell-Specific Control with AAV-M_3D, AAV-M_4D

4.1 Materials

4.1.1 Stereotaxic Equipment

1. Stereotaxic frame, mouse nose bar (Model 926) and rat ear bars (model 855) produced by David Kopf Instruments.
2. Stereotaxic drill and drill bits.
3. Stereotaxic cannula holder (Model 1776-P1) produced by David Kopf Instruments.
4. Various surgical instruments: scalpel, forceps, etc. (Fine Science Tools).
5. 10 μl Hamilton microsyringes (Model 7002KH) connected with Tygon tubing (0.02 mm i.d.) to injector cannula (33 gauge) produced my Plastics One Inc.
6. Small animal clippers.
7. Various surgical supplies: gauze, cotton tip applicators, betadine surgical scrub, nitrile gloves, etc.
8. Isoflurane for anesthesia (Sigma-Aldrich).
9. Temperature-regulated heating pad (e.g., TC-1000; CWE Inc., New York, NY).
10. Syringe pump.
11. Mineral oil.

4.1.2 Equipment Needed for Behavioral Testing of Open-Field Locomotion

1. Open-field arena(s) (measuring $31 \times 31 \times 31$ cm).
2. Video camera suspended above open-field arena(s).
3. Video tracking software (e.g., Noldus Ethovision V7.0 (Groningen, Netherlands)).

4.1.3 Materials for HSV-M_5 Transfections in M_5-KO or WT Mice

1. M_5-KO mice and wild-type controls (CD1/129).
2. M_5-HSV-GFP and M_5-control-GFP (see Note 5 for details on HSV vectors).
3. Morphine sulfate pentahydrate (Sigma, St. Louis, MO) (Note 6).

4.1.4 Materials for AAV-M3D or M4D Transfections in GAD2::Cre Mice

1. GAD2::Cre mice (Jackson Laboratory, $Gad2^{tm2(cre)Zjh}$/J, 010802).
2. AAV-FLEX-M_3D-mCherry or AAV-FLEX-M_4D-mCherry (see Note 7 for details on AAV vectors and DREADDs).
3. Morphine sulfate pentahydrate (Sigma, St. Louis, MO) (Note 8).
4. Dimethyl sulfoxide (DMSO).
5. Clozapine-N-oxide (CNO) (Note 9).

4.2 Methods

4.2.1 Viral Transfections in Mice

1. Fill Hamilton syringe/Tygon tubing/injector cannula assembly with mineral oil (or water) (Note 10). Place filled Hamilton syringe into syringe-pump and eject 4–10 μl. Wipe tip of injector, and withdraw 0.5–1.0 μl to create an air bubble. Place injecNor cannula into virus solution, and slowly load vector (rate of 0.1–3.0 μl/min). To conserve virus, consider loading enough viral vector to perform several surgeries (Note 11).
2. Anesthetize mice based on an approved Institutional Animal Care and Use Committee (IACUC) protocol. Anesthesia should be induced at 3 % isoflurane and maintained at 1.5 % isoflurane delivered via a vaporizer at 0.7 l/min O_2.
3. Secure mouse in a stereotaxic frame. Maintain body temperature at 37 ± 0.5 °C with a temperature-regulated heating pad.
4. Drill burr holes into the skull above the brain area of interest large enough to accommodate an injector cannula. Slowly lower injectors into burr holes to desired D/V coordinates into site of interest.
5. Begin injecting virus slowly (0.1–3.0 μl/min) until the desired volume of the virus has been dispensed 0.1–1.0 μl of virus. Note: volume and rate of injection can depend on specific type of virus, titer, desired spread, and limitations of syringe pump.
6. Allow for the injector cannula to remain in place for an additional 5–10 min to ensure vector diffusion.
7. Following diffusion period, slowly raise the cannula out of the skull.
8. Depending on experimental design, repeat steps 5–7 for alternate hemisphere or additional sites.
9. Once all viral injections are complete, retract the cannula, suture the wound, and apply standard post-operative care.
10. Depending on biosafety protocol, segregate cages from colony under HEPA-filtered cage tops for 48 h.

4.2.2 Behavioral Testing: Open-Field Locomotion

Open-field locomotion is a reliable measure of drug effect in rodents. Drug-induced hyperactivity is easy to quantify and has been shown, in rodents, in response to several different drugs of abuse. This drug-elicited, goal-directed behavior is an adaptive survival mechanism to encourage exploration, and risk taking. Increases in drug-induced locomotion often reflect activation of the mesolimbic DA system. Thus, running can be taken as a behavioral index reflective of the functioning and integrity of the DA system [57].

While there are several other methods to measure open-field locomotion (automated photocell cages, scored by observation), here we will be discussing video-recorded trials and offline-scoring using Noldus Ethovision tracking software (Fig. 3a) [22, 50].

1. Behavioral experiments should always be carried out at the same time of the day taking into account that the animals show minimal motor activity around noon under a light regime with lights on from 6 a.m. to 6 p.m.
2. To ensure best results, perform open-field testing in a room with dim red lighting and with a 70 dB white-noise generator.
3. Assign mice to specific open-fields such that they are consistently tested in the same environment.
4. Before commencing tests, habituate mice to the open-field arenas. Place each mouse in the center of its open-field and allow it to freely explore the environment. It is recommended to habituate mice at least once before testing.
5. Begin test days with a brief habituation period (30–60 min). Place each mouse in the center of its open-field and video-record their behavior.
6. Briefly remove mice from open-fields and return them to individual cages. Using dry paper towel, lightly wipe down each open-field and remove any feces and urine. Do not use ethanol or any other cleaner as the odors may influence behavior.
7. Administer injections to each mouse, before returning them to the center of their open-field. Begin recording video for the duration of your test phase.
8. If mice are performing additional tests on that day, repeat steps 6–7. When mice have completed testing, return them to their home cages and housing room.
9. Analyze videos using software (e.g., Noldus Ethovision) and calculate the measures of interest (horizontal distance traveled, rotations, etc.).

4.2.3 HSV-M_5 Transfections

A Herpes simplex viral vector (HSV) was used to transfect M_5 DNA [58] in a small field, to precisely define neurons causing the behavioral changes [59, 60] (Fig. 2d). Due to the time course of the HSV transfections, an accelerated testing period was required as maximal gene expression for HSV vectors occurs 24–72 h following infusion [59, 61]. M_5-KO and WT mice were run in groups of 4–6 mice over a period of 5 days [22]. On day 1, surgery was performed and either the HSV-M_5-GFP or HSV-control-GFP vector was bilaterally infused (at a volume of 0.5 μl per hemisphere at 2.5 μl/min) into the VTA or RMTg (relative to bregma: VTA—AP: −3.40, ML: ±0.50, DV: −4.40; RMTg—AP: −3.90, ML: ±0.40, DV: −3.88 [62]. On day 2, mice received standard post-surgical treatment and were allowed the day to recover.

Behavioral testing occurred on days 3 and 4, and each day began with a 60-min habituation period. On day 3, following habituation, each mouse was briefly removed from its test box, received a saline injection and was immediately placed back in the

center of its box. Video recording occurred over the next 2 h to track saline-induced locomotion. After the 2 h trial, mice were again briefly removed from their boxes, injected with 10 mg/kg morphine i.p., and were returned to the center of their respective boxes. Again, video acquisition occurred for 2 h. Following the morphine trial, mice were returned to their home cages and returned to the housing room. On day 4, following habituation, mice were injected with 30 mg/kg i.p. morphine. Again, locomotion was recorded for a 2 h period after which, the mice were returned to their home cages in the housing room. In order to minimize order effects over the 2 consecutive test days, all mice received increasing morphine doses (0, 10, 30 mg/kg) with each subsequent test. Video recordings were scored using Noldus Ethovision V7.0 (Groningen, Netherlands), which calculated the distance traveled (in m) for each 15-min period.

4.2.4 AAV-M_3D or M_4D Transfections of RMTg in GAD2::Cre Mice

To study the locomotor effects of muscarinic signaling on RMTg GABA neurons, we transfected GAD2::Cre mice with genes encoding the mutant muscarinic receptors M_3D or M_4D specifically into RMTg GABA neurons [56, 63] using Cre-responsive adeno-associated viral vectors (AAV) [55].

GAD2::Cre mice received bilateral microinjections of either AAV-M3D or AAV-M4D vectors (at a volume of 0.2 μl per hemisphere at a rate of 0.1 μl/min) into the RMTg (relative to bregma: RMTg—AP: −3.90, ML: ±0.40, DV: −3.88) [62].

Behavioral testing began 4–5 weeks after AAV infusions and occurred on alternate days for a total of 6 sessions. Testing sessions began with each mouse placed in the center of its test box for 1-h habituation, then briefly removed for an i.p. injection and returned to its box for a 3-h test. Test sessions 1 and 4, however, served as no-injection control trials, where, following habituation, each mouse was removed from its box, briefly handled, and then returned for a 3-h test without any injection. On test days 2 and 3, mice received either saline/vehicle alone, or CNO (counterbalanced). On test days 5 and 6, mice received either morphine alone, or morphine with CNO (counterbalanced). Following each testing session, mice were returned to their home cages, then to the housing room. All test sessions were video-recorded using overhead digital cameras. Recordings were analyzed using Noldus Ethovision V7.0 (Groningen, Netherlands) to calculate total horizontal distance traveled for each 30-min period.

4.3 Notes

5. A cDNA containing the full-length reading frame of mouse M_5 receptor DNA (M_5R) was subcloned into the bi-cistronic amplicon vector p1005 (Fig. 2d). The resulting vector, HSV-M_5-GFP, contained mM_5R after the HSV-derived IE4/5 promoter along with the cDNA for green fluorescent protein (GFP) after a CMV promoter. Replication-deficient Herpes

simplex virus-derived particles were made from this vector as previously described [60]. A control virus (p1005), HSV-control-GFP was also constructed; this was identical to the HSV-M_5 with the M_5R gene excluded. Both viruses (M_5R-p1005 and p1005) had titers $>1 \times 10^8$ infectious units/ml.

6. Morphine sulfate pentahydrate dissolved in sterile saline and injected i.p. at a volume of 10 ml/kg body weight and concentrations of 10 mg/kg and 30 mg/kg calculated according to free base weight.
7. To selectively excite or inhibit RMTg GABA neurons in mice, we used two mutant muscarinic receptors, M_3D and M_4D, also known as DREADDS: Designer Receptors Exclusively Activated by Designer Drugs [56]. We employed a Cre recombinase-dependent, AAV expression system called the AAV-FLEX approach. The AAV-FLEX vector carries a reversed and double-floxed effector gene to enable specific expression in transgenic mice expressing Cre recombinase under the control of the GAD2 promoter. The coding sequences of the M_3D or M_4D DREADDs were linked to the fluorescent protein, mCherry, and packaged into a Cre recombinase-dependent AAV vector to allow expression of either M_3D or M_4D and mCherry fusion proteins. In the absence of Cre recombinase, transgenes (M_3D-mCherry or M_4D-mCherry) are inverted with respect to the promoter between two pairs of heterotypic, antiparallel loxP sites, and thus transgene expression is off. When introduced to Cre-expressing cells, however, the transgene orientation is inverted by Cre-mediated excision, leading to the activation of the trans-gene expression. These mutant receptors are designed to be activated by CNO which can be systemically administered. Further, these receptors have been evolved such that they do not respond to endogenous ACh [64]. These receptors are identical to M_3 and M_4 muscarinic receptors except they both have the same 2 point mutations in the ACh binding site [65].
8. Morphine sulfate pentahydrate dissolved in sterile saline and injected i.p. at a volume of 10 ml/kg body weight and concentration of 10 mg/kg calculated according to free base weight.
9. CNO was dissolved in 0.5 % DMSO in sterile saline and injected i.p. at a volume of 10 ml/kg body weight for a final concentration of 2 mg/kg. CNO was generously donated through the National Institute of Mental Health's Chemical Synthesis and Drug Supply Program (Bethesda, MD).
10. Both mineral oil and water can be used to fill the assembly. Mineral oil is preferred, however, due to its greater viscosity and increased accuracy.

11. Depending on length of surgery, and properties of the viral vector, injectors may be loaded with enough vector for multiple sites and/or surgeries. If pursuing this option, ensure to load injector with excess vector. After infusing virus into first animal, wipe injector with ethanol, dry injector, and withdraw an additional air bubble (1.0 μl). Before beginning the following surgery, push out a volume greater than the withdrawn air bubble (e.g., 1.2 μl) to ensure that virus is correctly loaded at tip of injector.

5 Conclusions

M_2 and M_4 receptors directly inhibit LDT and PPT cholinergic neurons mediating arousal. Chronoamperometry studies in M_5 knockout mice show that activation of PPT/LDT cholinergic inputs to the midbrain results in sustained activation of dopamine neurons mainly via M_5 receptors. Behavioral studies in which M_5 receptors are downregulated (i.e., oligonucleotides or gene knockout) or upregulated (i.e., HSV M_5 transfection) show that M_5 receptors critically mediate sustained arousal and reward-seeking in response to brain-stimulation, food, and opioid rewards. These dopamine and cholinergic neuron populations are both inhibited by VTA and RMTg GABA neurons. RMTg GABA neurons express inhibitory M_4 and μ-opioid receptors that work together to disinhibit cholinergic and dopamine neurons in arousal states [55]. GFP-labeled transfections of these neurons with specific HSV- or AAV-muscarinic genes allows for studying the behavioral effects of inhibiting or activating these neurons using Cre lines and clozapine nitric oxide.

Acknowledgements

We thank our many collaborators and coauthors, including Gina Forster and Anthony Miller (electrochemistry), Haoran Wang, Sheena Josselyn, and Asim Rashid (HSV-M_5), Jun Chul Kim and Bryan Roth (AAV-M_3D and AAV-M_4D), and Junichi Takeuchi, Zheng-ping Jia, John Roder, and Juergen Wess (knockouts).

References

1. Bonner TI, Young AC, Brann MR, Buckley NJ (1988) Cloning and expression of the human and rat m5 muscarinic acetylcholine receptor genes. Neuron 1:403–410
2. Yeomans JS (2012) Muscarinic receptors in brain stem and mesopontine cholinergic arousal functions. Handb Exp Pharmacol 208:243–259
3. Yasuda RP, Ciesla W, Flores LR, Wall SJ, Li M, Satkus SA, Weisstein JS, Spagnola BV, Wolfe BB (1993) Development of antisera selective for m4 and m5 muscarinic cholinergic receptors: distribution of m4 and m5 receptors in rat brain. Mol Pharmacol 43: 149–157

4. Levey AI (1993) Immunological localization of m1-m5 muscarinic acetylcholine receptors in peripheral tissues and brain. Life Sci 52: 441–448
5. Vilaro MT, Palacios JM, Mengod G (1990) Localization of m5 muscarinic receptor mRNA in rat brain examined by in situ hybridization histochemistry. Neurosci Lett 114:154–159
6. Weiner DM, Brann MR (1989) The distribution of a dopamine D2 receptor mRNA in rat brain. FEBS Lett 253:207–213
7. Takeuchi J, Fulton J, Jia ZP, Abramov-Newerly W, Jamot L, Sud M, Coward D, Ralph M, Roder J, Yeomans J (2002) Increased drinking in mutant mice with truncated M5 muscarinic receptor genes. Pharmacol Biochem Behav 72:117–123
8. Yamada M, Lamping KG, Duttaroy A, Zhang W, Cui Y, Bymaster FP, McKinzie DL, Felder CC, Deng CX, Faraci FM, Wess J (2001) Cholinergic dilation of cerebral blood vessels is abolished in M(5) muscarinic acetylcholine receptor knockout mice. Proc Natl Acad Sci U S A 98:14096–14101
9. Redgrave P, Horrell RI (1976) Potentiation of central reward by localised perfusion of acetylcholine and 5-hydroxytryptamine. Nature 262: 305–307
10. Bauco P, Wise RA (1994) Potentiation of lateral hypothalamic and midline mesencephalic brain stimulation reinforcement by nicotine: examination of repeated treatment. J Pharmacol Exp Ther 271:294–301
11. Yeomans JS, Kofman O, McFarlane V (1985) Cholinergic involvement in lateral hypothalamic rewarding brain stimulation. Brain Res 329:19–26
12. Blaha CD, Allen LF, Das S, Inglis WL, Latimer MP, Vincent SR, Winn P (1996) Modulation of dopamine efflux in the nucleus accumbens after cholinergic stimulation of the ventral tegmental area in intact, pedunculopontine tegmental nucleus-lesioned, and laterodorsal tegmental nucleus-lesioned rats. J Neurosci 16:714–722
13. Yeomans JS, Baptista M (1997) Both nicotinic and muscarinic receptors in ventral tegmental area contribute to brain-stimulation reward. Pharmacol Biochem Behav 57:915–921
14. Yeomans JS, Takeuchi J, Baptista M, Flynn DD, Lepik K, Nobrega J, Fulton J, Ralph MR (2000) Brain-stimulation reward thresholds raised by an antisense oligonucleotide for the m5 muscarinic receptor infused near dopamine cells. J Neurosci 20:8861–8867
15. Sharf R, McKelvey J, Ranaldi R (2006) Blockade of muscarinic acetylcholine receptors in the ventral tegmental area prevents acquisition of food-rewarded operant responding in rats. Psychopharmacology (Berl) 186: 113–121
16. Rezayof A, Nazari-Serenjeh F, Zarrindast MR, Sepehri H, Delphi L (2007) Morphine-induced place preference: involvement of cholinergic receptors of the ventral tegmental area. Eur J Pharmacol 562:92–102
17. Rada PV, Mark GP, Yeomans JS, Hoebel BG (2000) Acetylcholine release in ventral tegmental area by hypothalamic self-stimulation, eating, and drinking. Pharmacol Biochem Behav 65:375–379
18. Mesulam MM, Mufson EJ, Wainer BH, Levey AI (1983) Central cholinergic pathways in the rat: an overview based on an alternative nomenclature (Ch1-Ch6). Neuroscience 10: 1185–1201
19. Oakman SA, Faris PL, Kerr PE, Cozzari C, Hartman BK (1995) Distribution of pontomesencephalic cholinergic neurons projecting to substantia nigra differs significantly from those projecting to ventral tegmental area. J Neurosci 15:5859–5869
20. Oakman SA, Faris PL, Cozzari C, Hartman BK (1999) Characterization of the extent of pontomesencephalic cholinergic neurons' projections to the thalamus: a comparison with projections to midbrain dopaminergic neurons. Neuroscience 94:529–547
21. Watabe-Uchida M, Zhu L, Ogawa SK, Vamanrao A, Uchida N (2012) Whole-brain mapping of direct inputs to midbrain dopamine neurons. Neuron 74:858–873
22. Wasserman DI, Wang HG, Rashid AJ, Josselyn SA, Yeomans JS (2013) Cholinergic control of morphine-induced locomotion in rostromedial tegmental nucleus versus ventral tegmental area sites. Eur J Neurosci 38:2774–2785
23. Isa T, Hall WC (2009) Exploring the superior colliculus in vitro. J Neurophysiol 102: 2581–2593
24. Dean P, Redgrave P, Westby GW (1989) Event or emergency? two response systems in the mammalian superior colliculus. Trends Neurosci 12:137–147
25. Steriade M, Datta S, Paré D, Oakson G, Curró Dossi RC (1990) Neuronal activities in brainstem cholinergic nuclei related to tonic activation processes in thalamocortical systems. J Neurosci 10:2541–2559
26. Paré D, Steriade M, Deschênes M, Bouhassira D (1990) Prolonged enhancement of anterior thalamic synaptic responsiveness by stimulation of a brain-stem cholinergic group. J Neurosci 10:20–33

27. McCormick DA (1992) Neurotransmitter actions in the thalamus and cerebral cortex and their role in neuromodulation of thalamocortical activity. Prog Neurobiol 39:337–388
28. Semba K, Fibiger HC (1992) Afferent connections of the laterodorsal and the pedunculopontine tegmental nuclei in the rat: a retro- and antero-grade transport and immunohistochemical study. J Comp Neurol 323:387–410
29. Manns ID, Alonso A, Jones BE (2000) Discharge properties of juxtacellularly labeled and immunohistochemically identified cholinergic basal forebrain neurons recorded in association with the electroencephalogram in anesthetized rats. J Neurosci 20:1505–1518
30. Dringenberg HC, Olmstead MC (2003) Integrated contributions of basal forebrain and thalamus to neocortical activation elicited by pedunculopontine tegmental stimulation in urethane-anesthetized rats. Neuroscience 119: 839–853
31. Lepore M, Franklin KB (1996) N-methyl-D-aspartate lesions of the pedunculopontine nucleus block acquisition and impair maintenance of responding reinforced with brain stimulation. Neuroscience 71:147–155
32. Bechara A, van der Kooy D (1989) The tegmental pedunculopontine nucleus: a brainstem output of the limbic system critical for the conditioned place preferences produced by morphine and amphetamine. J Neurosci 9: 3400–3409
33. Leonard CS, Llinás R (1994) Serotonergic and cholinergic inhibition of mesopontine cholinergic neurons controlling REM sleep: an in vitro electrophysiological study. Neuroscience 59:309–330
34. Kohlmeier KA, Ishibashi M, Wess J, Bickford ME, Leonard CS (2012) Knockouts reveal overlapping functions of M(2) and M(4) muscarinic receptors and evidence for a local glutamatergic circuit within the laterodorsal tegmental nucleus. J Neurophysiol 108: 2751–2766
35. Chapman CA, Yeomans JS, Blaha CD, Blackburn JR (1997) Increased striatal dopamine efflux follows scopolamine administered systemically or to the tegmental pedunculopontine nucleus. Neuroscience 76:177–186
36. Yeomans JS, Mathur A, Tampakeras M (1993) Rewarding brain stimulation: role of tegmental cholinergic neurons that activate dopamine neurons. Behav Neurosci 107:1077–1087
37. Mathur A, Shandarin A, LaViolette SR, Parker J, Yeomans JS (1997) Locomotion and stereotypy induced by scopolamine: contributions of muscarinic receptors near the pedunculopontine tegmental nucleus. Brain Res 775:144–155
38. Forster GL, Blaha CD (2000) Laterodorsal tegmental stimulation elicits dopamine efflux in the rat nucleus accumbens by activation of acetylcholine and glutamate receptors in the ventral tegmental area. Eur J Neurosci 12: 3596–3604
39. Tzavara ET, Bymaster FP, Davis RJ, Wade MR, Perry KW, Wess J, McKinzie DL, Felder C, Nomikos GG (2004) M4 muscarinic receptors regulate the dynamics of cholinergic and dopaminergic neurotransmission: relevance to the pathophysiology and treatment of related CNS pathologies. FASEB J 18:1410–1412
40. Forster GL, Blaha CD (2003) Pedunculopontine tegmental stimulation evokes striatal dopamine efflux by activation of acetylcholine and glutamate receptors in the midbrain and pons of the rat. Eur J Neurosci 17:751–762
41. Forster GL, Yeomans JS, Takeuchi J, Blaha CD (2001) M5 muscarinic receptors are required for prolonged accumbal dopamine release after electrical stimulation of the pons in mice. J Neurosci 22:RC190
42. Steidl S, Miller AD, Blaha CD, Yeomans JS (2011) M_5 muscarinic receptors mediate striatal dopamine activation by ventral tegmental morphine and pedunculopontine stimulation in mice. PLoS One 6:e27538
43. Ohno K, Hondo M, Sakurai T (2008) Cholinergic regulation of orexin/hypocretin neurons through M(3) muscarinic receptor in mice. J Pharmacol Sci 106:485–491
44. Michel FJ, Robillard JM, Trudeau LE (2004) Regulation of rat mesencephalic GABAergic neurones through muscarinic receptors. J Physiol 556:429–445
45. Blaha CD, Phillips AG (1996) A critical assessment of electrochemical procedures applied to the measurement of dopamine and its metabolites during drug-induced and species-typical behaviors. Behav Pharmacol 7:675–708
46. Kawagoe KT, Zimmerman JB, Wightman RM (1993) Principles of voltammetry and microelectrode surface states. J Neurosci Methods 48:225–240
47. Blaha CD, Lane RF (1983) Chemically modified electrode for in vivo monitoring of brain catecholamines. Brain Res Bull 10:861–864
48. Basile AS, Fedorova I, Zapata A, Liu X, Shippenberg T, Duttaroy A, Yamada M, Wess J (2002) Deletion of the M5 muscarinic acetylcholine receptor attenuates morphine reinforcement and withdrawal but not morphine analgesia. Proc Natl Acad Sci U S A 99: 11452–11457
49. Fink-Jensen A, Fedorova I, Wortwein G, Woldbye DP, Rasmussen T, Thomsen M, Bolwig TG, Knitowski KM, McKinzie DL,

Yamada M, Wess J, Basile A (2003) Role for M5 muscarinic acetylcholine receptors in cocaine addiction. J Neurosci Res 74:91–96

50. Steidl S, Yeomans JS (2009) M5 muscarinic receptor knockout mice show reduced morphine-induced locomotion but increased locomotion after cholinergic antagonism in the ventral tegmental area. J Pharmacol Exp Ther 328:263–275
51. Schmidt LS, Miller AD, Lester DB, Bay-Richter C, Schülein C, Frikke-Schmidt H, Wess J, Blaha CD, Woldbye DP, Fink-Jensen A, Wortwein G (2010) Increased amphetamine-induced locomotor activity, sensitization, and accumbal dopamine release in M5 muscarinic receptor knockout mice. Psychopharmacology (Berl) 207(4):547–558
52. Miller AD, Forster GL, Yeomans JS, Blaha CD (2005) Midbrain muscarinic receptors modulate morphine-induced accumbal and striatal dopamine efflux in the rat. Neuroscience 136:531–538
53. Forster GL, Falcon AJ, Miller AD, Heruc GA, Blaha CD (2002) Effects of laterodorsal tegmentum lesions on behavioral and dopamine responses evoked by morphine and d-amphetamine. Neuroscience 114:817–823
54. Jhou TC, Xu SP, Lee MR, Gallen CL, Ikemoto S (2012) Mapping of reinforcing and analgesic effects of the mu opioid agonist endomorphin-1 in the ventral midbrain of the rat. Psychopharmacology (Berl) 224:303–312
55. Wasserman DW, Tan JM, Kim J, Yeomans JS (2014) Muscarinic control of rostromedial tegmental nucleus GABA neurons and morphine-induced locomotion. Poster presented at Society for Neuroscience, Washington, D.C., 15–19 November 2014.
56. Rogan SC, Roth BL (2011) Remote control of neuronal signaling. Pharmacol Rev 63: 291–315
57. Tzschentke TM (2001) Pharmacology and behavioral pharmacology of the mesocortical dopamine system. Prog Neurobiol 63:241–320
58. Neve RL, Geller AI (1995) A defective herpes simplex virus vector system for gene delivery into the brain: comparison with alternative gene delivery systems and usefulness for gene therapy. Clin Neurosci 3:262–267
59. Carlezon WA, Boundy VA, Haile CN, Lane SB, Kalb RG, Neve RL, Nestler EJ (1997) Sensitization to morphine induced by viral-mediated gene transfer. Science 277:812–814
60. Han JH, Kushner SA, Yiu AP, Hsiang HLL, Buch T, Waisman A, Bontempi B, Neve RL, Frankland PW, Josselyn SA (2009) Selective erasure of a fear memory. Science 323: 1492–1496
61. Liu M, Thankachan S, Kaur S, Begum S, Blanco-Centurion C, Sakurai T, Yanagisawa M, Neve R, Shiromani PJ (2008) Orexin (hypocretin) gene transfer diminishes narcoleptic sleep behavior in mice. Eur J Neurosci 28: 1382–1393
62. Franklin KBJ, Paxinos G (2007) The mouse brain stereotaxic coordinates, 3rd edn. Academic, San Diego, CA
63. Taniguchi H, He M, Wu P, Kim S, Paik R, Sugino K, Kvitsiani D, Fu Y, Lu J, Lin Y, Miyoshi G, Shima Y, Fishell G, Nelson SB, Huang ZJ (2011) A resource of Cre driver lines for genetic targeting of GABAergic neurons in cerebral cortex. Neuron 71:995–1013
64. Armbruster BN, Li X, Pausch MH, Herlitze S, Roth BL (2007) Evolving the lock to fit the key to create a family of G protein-coupled receptors potently activated by an inert ligand. Proc Natl Acad Sci U S A 104:5163–5168
65. Wess J, Eglen RM, Gautam D (2007) Muscarinic acetylcholine receptors: mutant mice provide new insights for drug development. Nat Rev Drug Discov 6:721–733